Towards an understanding of surface finishing with compliant tools using a fast and accurate simulation method

Julien Chaves-Jacob, Anthony Beaucamp, Wule Zhu, Daisuke Kono, Jean-Marc Linares

Towards an understanding of surface finishing with compliant tools using a fast and accurate simulation method

Julien Chaves-Jacob [a]*, Anthony Beaucamp [b], Wule Zhu [b], Daisuke Kono [b], Jean-Marc Linares [a]

[a] Aix Marseille Univ, CNRS, ISM, Inst Movement Sci, Marseille, France
[b] Department of Micro-Engineering, Kyoto University, Kyoto, Japan

* Corresponding author
E-mail address: julien.chaves-jacob@univ-amu.fr

Abstract

Surface finishing with compliant tools is a widely used technology that still relies heavily on the trial-and-error approach. To predict surface evolution, one should ideally consider the tool as a set of grains and take into account the cutting action of each grain. In practice, the small size of abrasives renders this approach unpractical for industrial application. In this paper, the various aspects playing a role in surface generation, from micro-scale abrasives to macro-scale tool deformation as well as the time-dependent nature of compliant processes, are rationalized and modelled in a Folding Space (FS) rather than a classic geometrical space. This approach drastically reduces the computation time, and is found to be quite realistic as in each position the tool shape is distorted, taking into account the compliance level between the tool and local surface topography. Firstly, the concept of FS and methodology for physical representation of surfaces and processing by compliant tools in the FS are detailed. Next, predictions from the finishing model are analyzed for a variety of compliant grinding and polishing tools typically used in industry. Experimental testing confirms the accuracy and usefulness of the proposed method. To conclude, the model is exploited to offer a better understanding of finishing operations with compliant tools, while the limits and future possibilities of FS simulation method are discussed.

Keywords: Finishing; Compliant Tools; Modelling

Highlights:

- The proposed method is comprehensive as it takes into account process parameters, the initial surface quality, abrasive grain distribution and deformation of the tool.
- A formula based on Hertz and Preston's equations is proposed that reflects variability of removal rate in the folding space model.
- Level of compliance, tool deformation and abrasive wear are all considered in the model.
- The speed of proposed method allows for large scale multiplication of simulation runs to analyse the variation of surface quality under finishing operations with parameter adjustments.

Nomenclature

C_{area} : cutting area in the folding plane of the considered path (mm^2)
C_{area}^{i} : cutting area for i^{th} path track in the folding plane of the considered path (mm^2)
D_{mean} : mean grain size diameter of the Gaussian grain distribution (mm)
D_{max} : maximum grain size diameter of the Gaussian grain distribution (mm)
d_{max} : for SAG tools, maximum height between a pellet and its neighbours (mm)
h_{mean} : average height of the surface in the considered path (mm)
k : number of standard deviations defining the maximum grain size
k_0, k_1 : coefficients of tool wear law
L_{cc} : perimeter length of the tool at the cutter contact point (mm)
ϕ_{tool} : tool footprint diameter length during influence function test (mm)
ϕ_{pellet} : for SAG tools, diameter of pellets (mm)
MG_{area} : area of micro-graph observation (mm^2)
n : number of elementary tool profiles for one rotation of the tool
N : rotation per minutes of the tool (rpm)
N_{grain} : number of active grains in considered sample
p : coefficient depending on tool type accounting for density of active grains
Q'^{i} : material removal rate of the i^{th} path (mm^3/min)
Q'_{TIF} : material removal rate determined from the tool influence function (mm^3/min)
t : processing time (min)
T_{offset}^{i} : tool offset of the i^{th} path (mm)
T_{offset_TIF} : tool offset used to generate the tool influence function (mm)
T_{offset} : nominal tool offset of the simulated operation (mm)
V_c : cutting speed of the simulated operation (m/min)
V_{c_TIF} : cutting speed to generate the tool influence function (m/min)
Vf : feed rate of the tool (mm/min)
Z : truncation value of the Gaussian grain distribution
σ : standard deviation of the Gaussian grain distribution (mm)

1. Introduction

Grinding and polishing are common and necessary finishing steps for numerous engineered parts. In contrast to rigid grinding process, compliant tools use a flexible support material to achieve a smooth connection between the tool position and the resulting contact force. Conventionally, polishing stages have been performed manually with hand operated spindles, but such work can be harmful to the health of the operator and may induce lung diseases [1]. Thus, the scientific community is making a concerted effort on automating these operations, such that they can become safe and cost-effective. To succeed in this aim, three goals have been pursued in particular.

The first goal is to identify machine tools with the potential for carrying out compliant finishing operations. Kakinuma et al. [2] developed prototypes of specialized 5-axis polishing machines, that are equipped with a control system able to regulate the tool inclination, position, and applied force. Their study highlights that increased control of both position and force improves the uniformity of roughness on the workpiece surface when compared with the more simplistic position only control. However, this also increases complexity of the machine and control system. To reduce the costs of specialized polishing machines, Nagata et al. [3] proposed to add a force control system on a common industrial 6-axis robot used to polish molds. The authors showed in this work that the proposed force control system is sufficiently powerful to carry out polishing operations successfully with an industrial robot, though the low overall stiffness of robots and the dynamic uncertainty of joint motion remain issues to be solved. Another method consists of using the same machine to realize rough milling of the workpiece followed by the polishing stages [4-6]. The advantages of this

approach are its low cost (mechanical workshops are typically equipped with such machinery) and the ability to keep the reference frame of the workpiece constant throughout the manufacturing steps. On the other hand, this method relies on the use of a conventional CNC machine with control in the position domain but no direct ability to adjust contact load.

The second goal is to determine suitable tools to carry out polishing operations. A flexible tool must be used to obtain a smooth connection between the tool position and resulting contact force. Geometric offsetting of a compliant tool into the workpiece surface directly affects the exerted pressure, and thus the local material removal rate of the polishing operation. Deyang et al. [4] established this relationship in the case of a polishing disk, by empirically obtaining the pressure field between the tool and the polished surface and using this data to predict material removal. The authors were interested in particular by the interaction between two adjacent paths and validated their results experimentally. Pessoles et al. [5] also used a passive abrasive disc mounted onto a suitable support to carry out polishing operations. A more detailed experimental procedure was used to calibrate the relationship between tool displacement and applied polishing force. The authors derived process prescriptions to polish an industrial injection mold and obtained similar polishing time and quality to the previously employed manual process, except in sharply curved corners where the obtained surface quality was lower. To explain this phenomenon, the authors commented on kinematic aspects of the CNC machine. Furthermore, the lack of direct force control when polishing operations are carried out on a common machine tool highlights the necessity to characterize the tool shape, so it can be taken into account in generation of the CNC toolpath. For this purpose, Chaves-Jacob et al. [6], proposed a method to adapt toolpaths to the tool shape. The method employs flank polishing with a toolpath composed of a carrier path and optimised pattern [7], such as repeating loops across the workpiece surface. To compensate for variations of the tool shape, the authors start by profiling the tool shape with a CNC laser facility and then compensate tool radius variations as the tool moves relative to the surface normal. This method requires very flexible tooling to control the exerted polishing pressure field. But this flexibility is usually achieved by using compliant materials that are less durable than the typical bond in grinding wheels, and so it can be detrimental to the tool lifetime. To combine the advantages of flexible tools without incurring such degradation of tool lifetime, Beaucamp et al. [8] proposed an innovative shape adaptive grinding tool composed of a flexible support material on top of which rigid pellets loaded with abrasives are affixed. Unlike loose abrasive polishing, the hard contact between the rigid pellets and workpiece surface allows for deterministic prediction of the removal action by abrasives embedded in the pellets [9]. An additional study [10] on the application of this tool to low-rigidity components was carried out to increase the accuracy of material removal distribution.

The third goal is the control and prediction of polishing results through simulation. Polishing operations are difficult to simulate due to the multiscale of involved phenomena. A polished surface is the compound result of a multitude of localized cutting actions on the workpiece by small grains. Furthermore, every one of these local cutting phenomena is influenced by the instantaneous condition of the workpiece surface, which is the combined result of previous cutting passes within the same polishing operation. Prediction methods published in the literature may be classified into three main types:

1. Empirical methods: These methods are based on prediction models obtained by best-fitting a mathematical equation to experimental results. This kind of model is most appropriate for interpolating process conditions within the boundaries of the realized tests, but generally cannot make useful and reliable predictions outside these boundaries.

2. Semi-empirical methods: These methods rely on a set of experiments to derive the behavior law between material removal and cutting conditions in an elementary case. Thereafter, this law is used to predict polishing results in a more complex case. For example, Cheung *et al.* [11] realized an elementary polishing

test at a discrete point (Tool Influence Function, TIF) to determine the elementary footprint of a polishing tool. Next, this elementary footprint was convoluted with a complex toolpath to predict the resulting polished surface. Lu et al. [12] used a TIF experiment in dual-axis wheel polishing to derive the topology of roughness in cases where either a single or dual-axis were used. Thereafter, the obtained result was translated along the toolpath to predict the final surface topography. Through this methodology, they concluded that dual-axis polishing homogenizes and reduces the generated surface roughness compared to single-axis wheel polishing. Going more in-depth, a probabilistic undeformed chip thickness model was proposed to enhance prediction of the surface roughness [13]. To predict the machined workpiece topography, process kinematics of single grains on the tool is usually considered [14-15].

3. Analytical methods: These methods attempt to consider most of the complex phenomena involved in the polishing process. Due to the multitude of local cutting phenomena and their interactions, it is difficult to obtain a realistic prediction of the polished surface. However, in cases where this type of method is carefully and thoughtfully implemented, they offer great possibilities for parameter change and can therefore estimate a large range of polishing conditions. One of the main objectives of this kind of method is to predict the finished surface parameters in terms of form, waviness and roughness. To achieve this, three classes of analytical methods have been described in the literature:
   - Class #1 is based on the nominal tool shape. This kind of method is very fast and simple to implement, but only provides a rough assessment of polishing results. Furthermore, this class is by definition limited to stiff tools and thus not well-suited to compliant polishing tools. For example, Denkena *et al.* [16] used this methodology to predict the surface roughness in 5-axis grinding operations. Zhang *et al.* [17] used another model to predict the profile roughness of internal tubes finished by a novel magnetic polishing process. In their simulation, the polishing tool is modeled as a rigid smooth circle, and the surface profile is modeled by a succession of parabolas to improve accuracy.
   - Class #2 considers the tool envelope profile. In this model, the tool feed rate is considered negligible when compared to the tool rotation rate. With this assumption, the tool surface may be considered as the revolution of a profile, which is the envelope of higher grains. This method can thus predict the surface roughness of ground or polished surfaces more accurately than Class #1. Uhlmann *et al.* [18] used a class #2 model to predict surface roughness in a 4-axis grinding operation.
   - Class #3 considers the tool as a set of grains and takes into account the cutting action of each grain. This method class is very accurate but requires a very long simulation time. This high level physical model is useful to study very specific problems. For example, Setti *et al.* [19] investigated the uncut chip thickness to understand the mechanism of surface generation in micro-grinding. To alleviate computations, they divided the tool and grinding phenomena into several slices in the axial direction, so as to convert the 3D problem into a series of 2D ones. Meanwhile, Darafon *et al.* [20] employed a similar methodology in full 3D, to determine the uncut chip thickness and obtain the instantaneous material removal rate. Like Darafon, Zang et al. [21] used this kind of method to determine the uncut chip thickness through a faster numerical algorithm and proceeded to study the influence of distribution and protrusion of grains. Furthermore, they demonstrated usage of this model to predict the surface roughness. In the work of Zhou *et Al.* [22], the loss of abrasive grains in tool wear was studied with a grain level model. It should be noted that models in this class have been mostly used to predict the evolution of surface roughness, while ignoring other surface quality parameters.

In this paper, an enhanced class #3 model is proposed that can predict the evolution of all surface quality parameters (form, waviness and roughness) for a wide range of compliant finishing tool types. One of the main characteristics of the proposed method is to carry out simulations not in a classic geometrical 3D space but in a 2D Folding Space (FS). This approach is used to reduce drastically the computation time and obtain an accurate prediction of the polishing result. Firstly, the FS method is presented and the physical aspects of polishing with their adaptation to the FS method are detailed. Actual implementation of the model is described in the next section: by realistically taking into account tool shape distortion as function of the tool type and surface topography, the method provides useful insights into the behavior of various finishing processes. Next, a set of experimental validation is carried out to ascertain reliability of the FS method. Finally, usefulness of the proposed model in understanding finishing operations with compliant tools is discussed, together with an analysis of the limitations and future opportunities of the method.

2. Folding space methodology

2.1. Basic concept

Full 3D simulations considering the interaction of each abrasive grain with the material (class #3 as defined in section 1) can be so time consuming that a few seconds of polishing simulation can amount to dozens or hundreds of computation hours. This partly explains why the experimental approach is still widely in use when dealing with compliant tools. Here, the computations relating to the 3D problem are carried out in a FS in order to considerably reduce the simulation time while maintaining a reasonable level of detail from the perspective of both workpiece surface and finishing process. Fig. 1 illustrates the FS method used to generate a representative profile from a workpiece surface measurement (shown in Fig. 1 a). In digital metrology processing, it is common for the surface to be filtered into three separate orders of defect: form, waviness and roughness. The associated filtering parameters are defined by ISO standards [23]. The FS method exploits this separation into three elementary surfaces, by finding the preferential orientation of each level of defect (U1, U2 and U3 in Fig. 1 b). Thereafter, an equivalent profile is associated with each filtered surface (see Fig. 1 c). The orientation of the equivalent profiles is based on topography of the starting surface condition and knowledge of the polishing process mechanics, such that they strongly correlate with pattern signature on the processed surface. Next, these three profiles are folded in the FS by summation in a common plane (S, Z), as shown in Fig. 1 d. By construction, this profile has the same surface parameter criteria as the initial surface in terms of form, waviness and roughness.

Form error is typically composed of a small number of features (usually one or two bumps, rarely more) whereas waviness and roughness are more typically made up of repeating patterns. For this reason, two different approaches are used to associate equivalent profiles:

- Form: the equivalent profile is selected to have approximately the same maximum height parameter ([24], Pt) as the elementary form surface ([25], St). Furthermore, the equivalent profile must have similar topology as the elementary form surface (a unique bump, two bumps or other specific shape).
- Waviness and roughness: the equivalent profiles have similar average period and arithmetical mean deviation (Wa and Ra parameters in current ISO ([24]) value as the associated elementary surfaces (Sa_w and Sa_R [25]). These profiles are defined over the same length as the equivalent form profile.

Main limitation of this method is the loss of the exact 3D topography of the surface. As the proposed method is not bijective, an infinity of surfaces may produce the same equivalent profile. However, as illustrated in Fig. 1 e), a representative 3D surface may be re-constructed by extruding in one direction the summation of form and waviness profiles, and in a perpendicular direction the roughness profile.

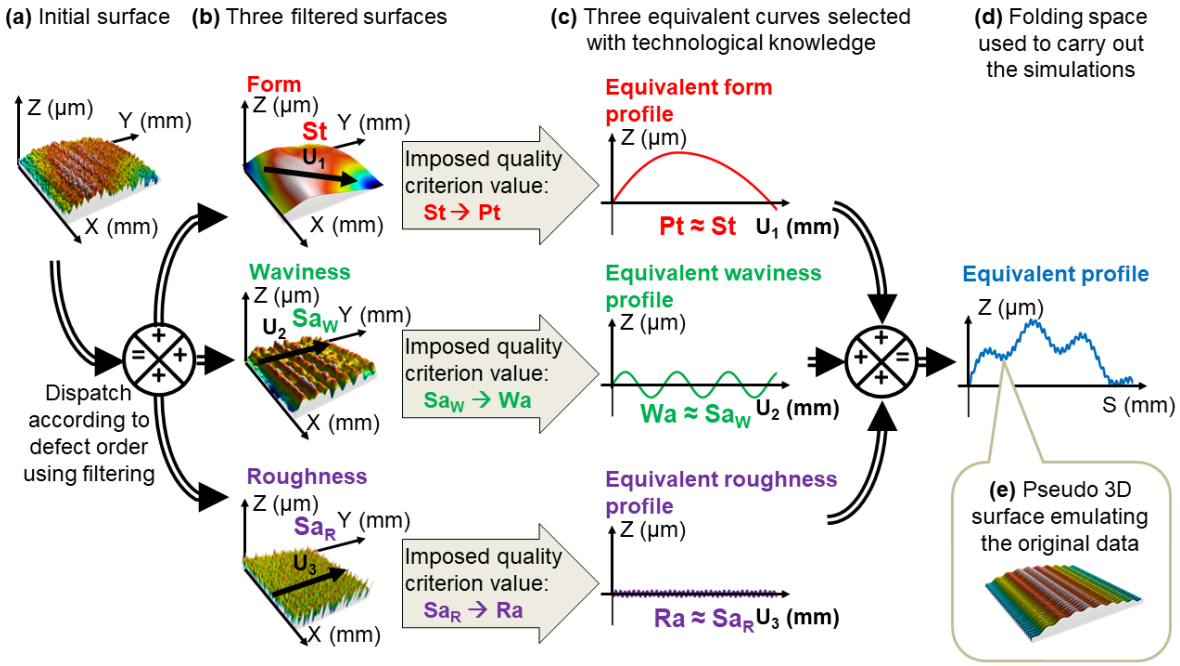

Fig. 1: Presentation of the folding space method; a) initial surface measurement in 3D, b) filtering of initial surface into three separate orders of defect: form, waviness and roughness, c) equivalent profile associated with each filtered surface, d) after summation, equivalent folding space profile of the initial 3D surface, e) pseudo 3D surface emulating the original data, reconstructed by inverting the numerical process.

2.2. Selection of main characteristic directions in polishing process

Fig. 2 highlights a polishing operation and two planes (marked in red and blue, respectively) specific to the process. Indeed, in polishing operations roughness defects are mainly generated in the plane C-C perpendicular to the cutting direction of grains (marked in red). In this type of operation, roughness is mainly generated by the envelope profile of the tool grains for one spindle rotation, and repeated along the tool path for each revolution of the tool. On the other hand, form and waviness defects are principally observed in the plane F-F, perpendicular to the tool feed (marked in blue). These defects are respectively caused by tool wear and variation of tool offsetting into the workpiece (which affects the area of contact) for the form, and by track spacing (lateral displacement between two passes) for the waviness. Using the folding method presented in section 2.1 these two planes are folded when carrying out the polishing simulation into the Folding Plane (FP).

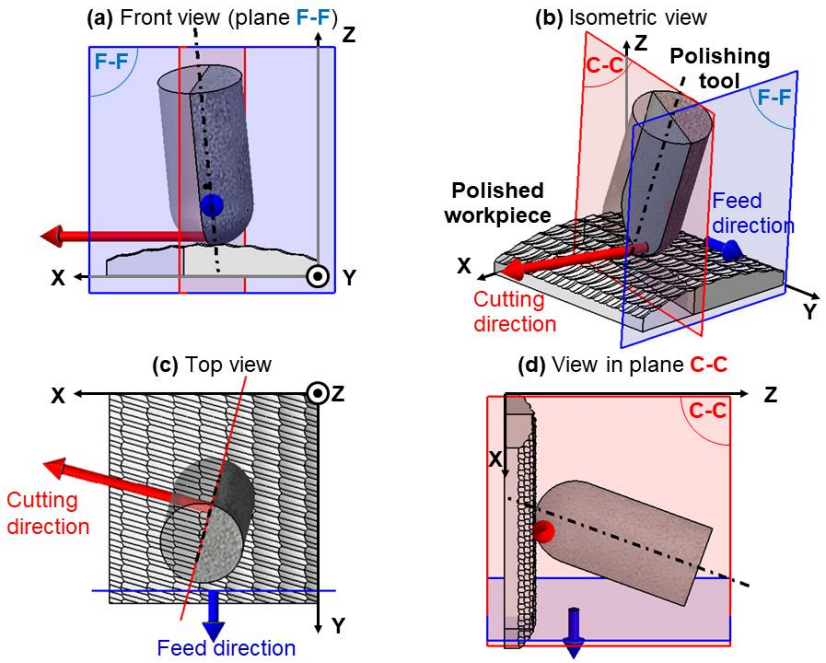

Fig. 2: Definition of the two main planes associated with defect generation in polishing operation: plane F-F (in blue) is perpendicular to the feed direction and plane C-C (in red) is perpendicular to the cutting direction. In particular: a) front view showing the plane where form and waviness phenomena occur, b) isometric view, c) top view, d) view in plane C-C where roughness phenomena occurs.

3. Conceptualization of finishing processes

3.1. Methodology: inputs/outputs

Fig. 3 presents the overall scope of the presented work. Both surface and tool are characterized by two profiles in the folded simulation plane. Thus, inputs to define the initial surface and tool profile must be provided together with information about the machining process:

- Inputs relative to the initial surface to generate the equivalent profile in the FP: surface topology and surface criteria (see section 2.1).
- Inputs relative to the tool: tool type (see section 3.4), tool shape and abrasives grain size distribution.
- Inputs relative to the machining process: cutting conditions (tool inclination, nominal tool offset, track spacing, spindle rotation speed and tool feed rate) and cutting rate of polishing tool (material removal rate Q'_{TIF}, and tool footprint diameter ϕ_{tool}).

Material removal is linked to specific values of the cutting speed (V_{c_TIF}) and tool offset penetration of flexible polishing tool into the workpiece (T_{offset_TIF}). Generally, these values (Q'_{TIF} and ϕ_{tool}) are obtained by generating an experimental Tool Influence Function (TIF: plunge test with tool spindle rotating). The measured footprint is used to determine both values. Output of method is a 2D profile in the FP, from which a pseudo-surface can be reconstructed and its associated quality criteria can be estimated. These can then be compared with experimental surface quality criteria.

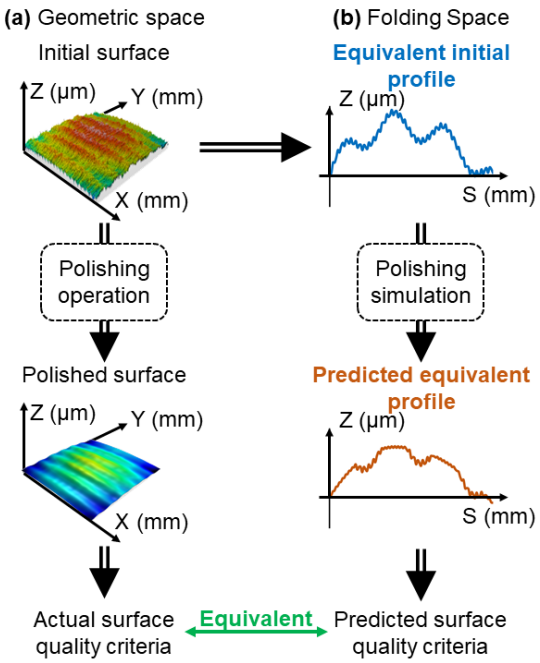

Fig. 3: Data flow, showing the measured surface quality before and after polishing being compared with that predicted by the proposed model: a) experiments b) simulations.

Fig.4 summarizes the successive steps in the polishing process model. Firstly, the provided inputs are used to generate an envelope of the undistorted tool and fold the starting surface profile. Thereafter, for each successive pass the tool profile is adapted to the evolving surface geometry at that stage. This adaptation varies according to the type of polishing tool. The local surface profile is also used to compute the actual tool offset and recalculate the actual material removal rate. After iterating through these stages, the compound removed material is computed and the actual material removal rate can be assessed. Next, the tool is displaced by one track space and the process starts again with the surface profile as cut by the previous pass.

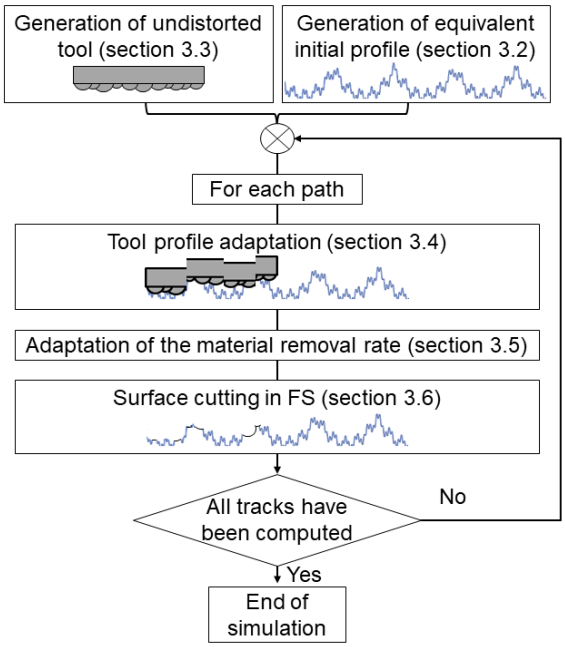

Fig. 4: Flowchart of proposed method with the main steps identified as: generation of the undistorted tool profile, adaption of the profile in terms of compliance and time-dependence, followed by actual surface cutting for each path.

3.2. Generation of equivalent initial profile

The folding method presented in section 2.1 is used to compute the equivalent initial profile. This is an important step of the proposed method, especially for the form profile component. For example, reducing the form error of a surface with a big central bump takes considerably longer by polishing process than polishing a flat surface with only a narrow peak in the middle (the necessary volume of material to be removed on these workpieces is not equivalent). To illustrate this, two different equivalent initial profiles associated with the later experimental validation (see section 5) are detailed here:

- Fig. 5 a) illustrates the generic profile for initial surfaces which have already received a rough polishing stage. In this case, the initial form profile is defined as a parabolic curve that represents rounding of the roughly polished surface.
- Fig. 5 b) shows the profile of a rough surface obtained by additive manufacturing using Selective Laser Melting (SLM) process. Rough surfaces associated with particular processes (milling, turning, additive manufacturing or other) require such specific form descriptions to improve accuracy of the initial representative profile. Experimental measurements were used to derive the repeating peaks in the form profile topology associated with this particular rough SLM surface. These peaks are the remnants of melted powder grains striding the melting pool. Indeed, the form defect of this kind of surface can be accurately represented by the sum of a bump profile (defined by a parabola) and a jagged profile (defined by succession of circular arcs of 15 mm radius and peak-to-valley height of 0.12 mm).

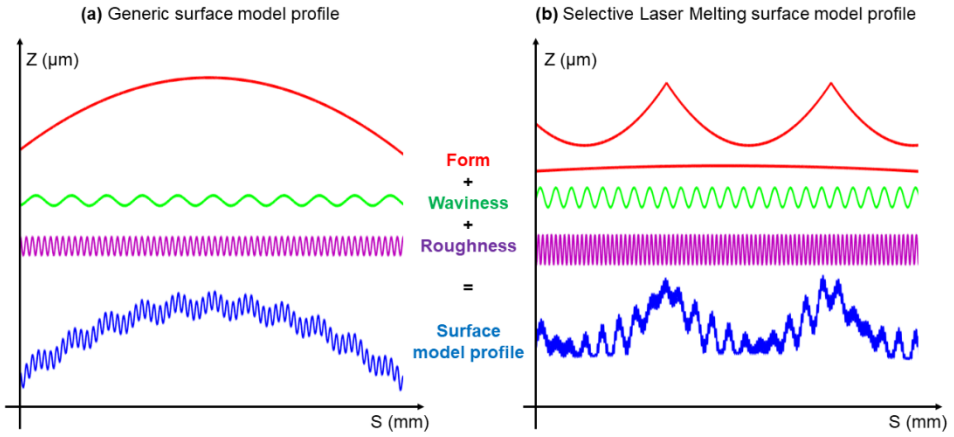

Fig. 5: Construction of equivalent initial profiles used in later validation: a) generic model for a surface that has already undergone rough polishing, b) specific model for a rough SLM surface.

3.3. Generation of undistorted tool profile

The tool is modelled by a profile in the FP. Liu et al. [26] demonstrated by simulation that the grain shape only has a minor effect on predicted roughness (grains considered in [26]: sphere, truncated cone and cone). Therefore, in this proposed method a sphere grain model is used for simplification. To model the stochastic nature of grain diameters, a Gaussian distribution is used. This distribution is controlled by a mean grain size diameter D_{mean} and standard deviation σ. These values are set in accordance with defined standards [27]. Furthermore, to limit the value of grain diameter which could be infinite in a theoretical

Gaussian distribution, a maximum grain size D_{max} is specified. This maximum value is specified relative to D_{mean} by a factor k times the standard deviation σ (Eq.1). The value of this k coefficient depends on the state of tool wear (see section 4.2)

$$D_{max} = D_{mean} + k \cdot \sigma \quad (1)$$

An elementary tool profile represents the active grains (grains that will touch the surface) in a plane containing the tool axis, as shown in Fig. 6 a). As proposed by Xi *et al.* [28], the elementary tool profile is a succession of half circles touching each other, the centres of which are aligned along a straight line.

In one rotation, numerous elementary tool profiles machine the workpiece. This number is noted n and is computed from Eq.2 as shown below. n mainly depends on the active tool perimeter (L_{cc}, linked to the tool geometry and tool inclination) and the mean grain diameter, D_{mean}. Furthermore, a coefficient p is added to take into account the density of active grains on the tool surface (a procedure to determine this coefficient is defined in section 4.1).

$$n = \frac{1}{p} * \frac{L_{cc}}{D_{mean}} \quad (2)$$

Fig. 6 presents the construction principle of undistorted tool profile from the elementary tool profiles (Fig. 6 a). In a first step, all the elementary tool profiles are superimposed, and the tool envelope profile is determined (Fig. 6 b). This tool profile envelope corresponds to the imprinted tool profile for one rotation (Fig. 6 c). Between each rotation, the tool covers a distance equal to the feed rate Vf, divided by the spindle rotation speed N. The tool profile for one rotation is repeatedly translated by this distance (Fig. 6 d) and the resulting envelope is used to define the undistorted tool profile (Fig. 6 e).

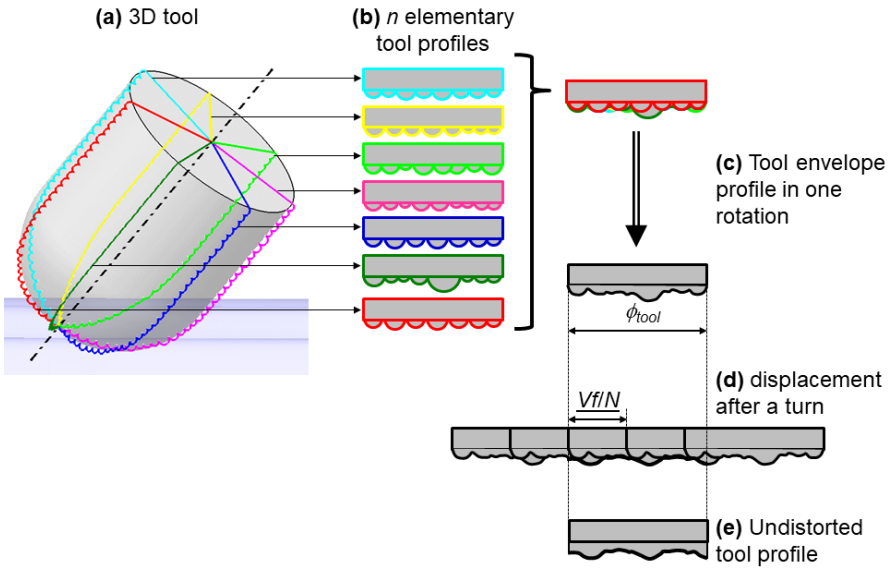

Fig. 6: Generation of the undistorted tool profile used to model the 3D polishing tool: a) overview of polishing tool in 3D, b) elementary tool profiles, c) superimposed tool envelopes profiles for one rotation, d) consideration of the feed rate, e) overall tool profile before surface adaptation.

3.4. Tool profile adaptation

As polishing tools are flexible, they will tend to deform and comply with the workpiece surface. Fig. 7 presents four different types of polishing tools considered in the method:

- Shape Adaptive Grinding (SAG): these tools [29] maintain general compliance with the surface thanks to a flexible support, but achieve a locally hard contact thanks to rigid pellets loaded with abrasive grains. These tools have a very high grinding ratio, and thus a long lifetime, with relatively high material removal rate.
- Abrasive caps: stiff abrasive sandpaper caps mounted on a flexible support. This type of tool cuts through the surface with a very high material removal rate. However, the grinding ratio is low so the tools have a short lifetime.
- Flexible wheels: polishing tool composed of abrasive grains embedded into a supple rubber matrix moulded around a stem. These tools have better surface compliance than abrasive caps, but relatively low material removal rate.
- Felts: soft polishing felt used with loose abrasive grains. These tools also have good surface compliance, but the lowest material removal rate as grains mainly roll across the workpiece surface.

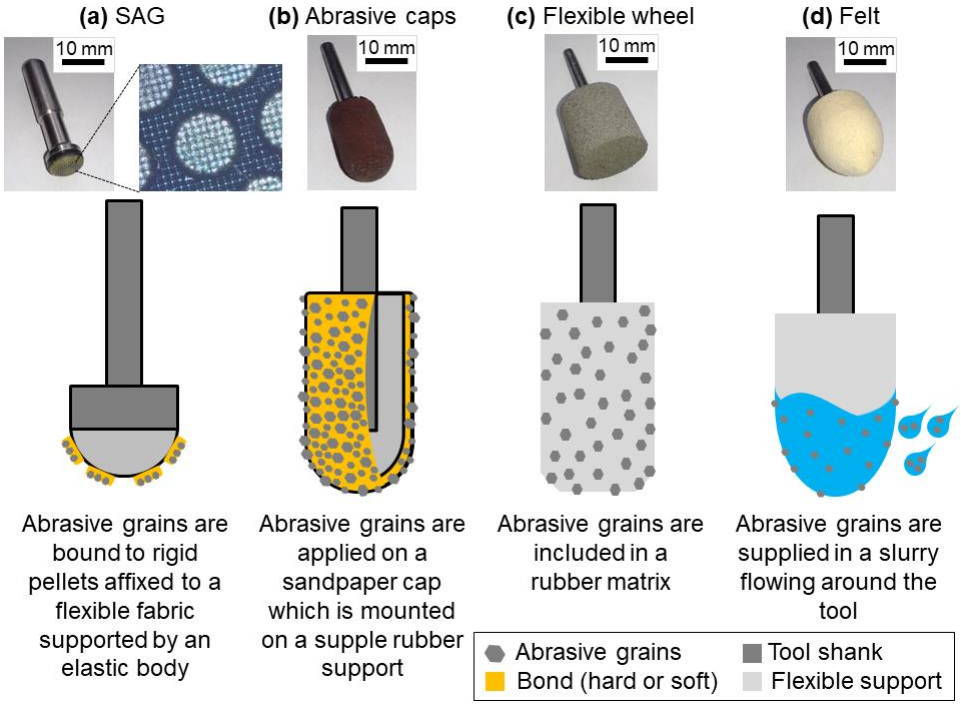

Fig. 7: Four tool types considered in the later validation of proposed method: a) shape adaptive grinding, b) abrasive cap, c) flexible wheel, d) felt.

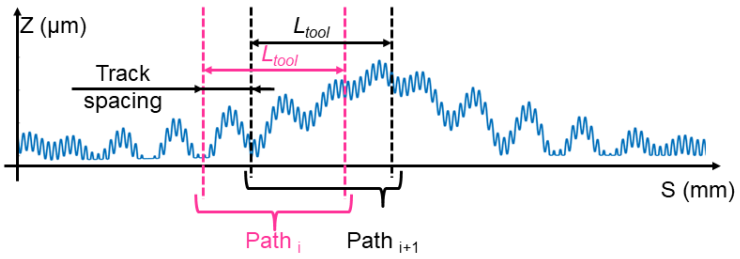

Fig. 8: Equivalent initial profile and position of successive simulated paths.

Each of the four considered tool types geometrically adapts differently to the locally polished surface. Fig. 8 presents the initial equivalent profile in FP. In this figure, the position of two consecutive path tracks are highlighted (path ^{i} and path $^{i+1}$). Each track is distant from the previous by a single track spacing increment. During the polishing simulation of one path, the tool may only remove material in a zone of length ϕ_{tool}. Note that profile figures are presented with a great anamorphosis (Z axis in µm and S axis in mm), which gives the impression of great sloping angles along the profile, while in fact these angles are minute.

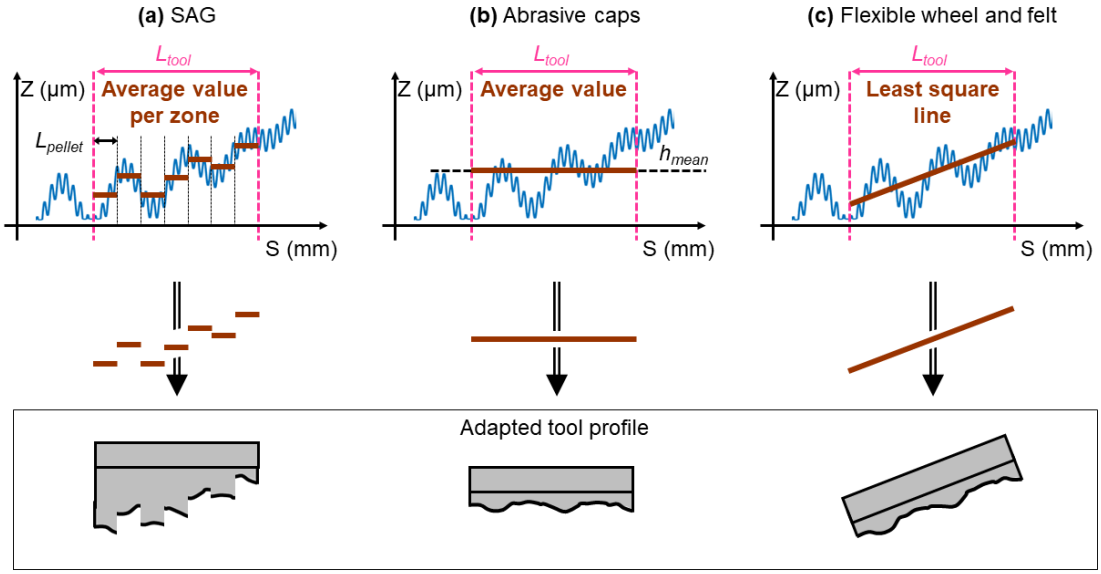

Fig. 9: Tool specific profile adaptation models: a) zonal averaging for shape adaptive grinding, b) overall averaging for abrasive caps, c) and least-square line for flexible wheel and felt (diagrams are presented with great anamorphosis;, Z-axis in µm and S-axis in mm).

Fig. 9 presents the level of surface adaptation for each of the tool types considered:

- SAG is a hybrid tool, simultaneously globally flexible with its elastic support and locally rigid thanks to its rigid pellets. The structure of SAG tools comprises a metal mesh constraining the maximum deviation between a pellet and its immediate neighbours, d_{max}. This maximum deviation value was estimated to be around 25 µm, by finite element analysis of the hyper-elastic material and mesh deformation under compression. Therefore, the initially undistorted SAG tool profile is deformed by a succession of horizontal strain lines with a length of ϕ_{pellet} = 0.5 mm. The maximal vertical deviation between strain lines is d_{max}. Each strain line adapts, as best as possible, to the profile portion where it is located while respecting these previous constraints (Fig. 9 a).

- Abrasive caps are the most rigid polishing tool considered in this study. Nominal tool geometry is a hemisphere, but tool wear very quickly changes the local shape into a cone frustum. In the plane perpendicular to the cutting speed, this cone is modelled as a horizontal strain line. Therefore, the abrasive cap tool profile remains undistorted in the simulation (Fig. 9 b).

- Flexible wheels and felts are the most flexible tools of this study. Unlike the SAG tools, this kind of tool easily deform in accordance with protruding surface peaks, thus they are modelled as a least square line of the profile portion where they are located (Fig. 9 c).

3.5. Adaptation of material removal rate

As input of the method, the material removal rate is also required. Usually a reference value $Q'_{\_TIF}$ is obtained by generating an experimental Tool Influence function (TIF) for a given cutting speed V_{c_TIF} and tool offset T_{offset_TIF}. Thereafter, the influence of cutting speed and tool offset variation on the material removal rate can be modelled.

In polishing, the tool is flexible and this property is used to smoothly link the applied force to the machine displacement. In this kind of operation the tool offset, or tool engagement, is one of the main parameter of the process. During a polishing operation, the variation of surface height will change the tool offset value. In the considered path the surface has an average height of h_{mean}. Thus the tool offset of i^{th} path, ${T_{offset}}^{i}$, is defined by Eq. 3.

$$ {T_{offset}}^{i} = T_{offset} + h_{mean} \tag{3} $$

With T_{offset} the nominal tool offset of simulated operation.

On the other hand, Preston's law [30] highlights that the removal rate is proportional to the average abrasive cutting speed and pressure. Firstly, the variation in cutting speed between the value used to generate the TIF and the one used in the simulation is expressed as a simple fraction affecting removal rate in Eq. 4. Secondly, variation of tool offset will influence the tool/workpiece contact pressure. Hertz theory for a sphere contacting a half-space shows that the pressure variation is proportional to the tool offset raised to the power of 0.5 [31]. These observations are combined to derive the material removal rate modulation as function of the cutting speed and local tool engagement (Eq. 4.).

$$ {Q'}^{i} = {Q'}_{TIF} \cdot \left(\frac{V_c}{V_{C\_TIF}} \right) \left(\frac{{T_{offset}}^{i}}{T_{offset\_TIF}} \right)^{0.5} \tag{4} $$

In the introduction, the issue of machine accuracy when implementing polishing processes was mentioned. As seen in Eq. 4, the material removal rate is linked to the tool offset. If a machine suffers from a lack of positional accuracy this will convert into a variation of tool offset in-process. Such variation can induce form/waviness defects on the workpiece. Defects may be positive (undercut) or negative (overcut) relative to the nominal geometry. The proposed method may be used to simulate the effects of such positional errors. This is carried out with two simulations: with/without machine error. Machine position errors may be classified in two types: systematic and random. Systematic errors could be modelled through progressive drift of the offset value (from track to track), whilst random errors could be modelled through random variation of the offset value (from track to track). Consequently, the difference between these two simulations provides an indicator of the impact of machine inaccuracy on the polishing performance. A similar approach may be used to predict the variation of surface finish in corrective process, in which a prescribed regime for the tool offset and advance feed are used, instead of constant values.

3.6. Surface abrasion in folding space

In the simulation plane, material to be removed appears as an abrasion area between the distorted profile and workpiece surface profile. This area is obtained when dividing the material removal rate (determined in Eq. 4) by the tool feed rate (Eq. 5):

$$ {C_{area}}^{i} = \left(\frac{{Q'}^{i}}{V_f} \right) \tag{5} $$

As shown in Fig. 10, the adapted tool is positioned on top of the profile and displaced down until the area between the tool and profile corresponds to the calculated abrasion area (Eq. 5). With the tool in this position, the intersecting area represents material removed for one track of the tool path.

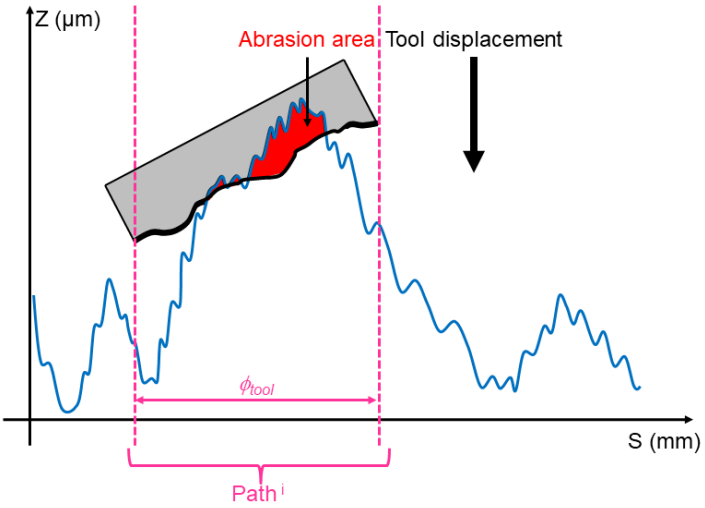

Fig. 10: An iterative method based on calculation of the abrasion area is used to determine the vertical position of adapted tool profile, ensuring that the exact amount of material is removed for each path track.

4. Experimental determination of method parameters

4.1. Determination of active grains on tool surface: *p*

According to the tool type, the number of active grains on the surface of the tool may vary. To take this into account, the coefficient *p* was added in Eq. 2. This coefficient represents the proportion of area occupied by active grain on the surface of tool relative to the entire tool surface area.

A method to experimentally estimate this value consists of taking micro-graphs of the representative active surface of the tool and counting the number of active grains in the measured area. The *p* coefficient is estimated as the average surface area occupied by active grains divided by the surface area of the micro-graph (Eq. 6). Fig. 11 illustrates this method on two different types of tools. In this case, manual determination and counting of the active grains was carried out; naturally, an image recognition algorithm may be used to simplify the operation. In Fig. 11 the active grains are surrounded by a green square with a lateral size equal to the mean grain size diameter. In the case of SAG tools, several pellets must be included in the area of measurement to obtain an average value.

$$p = \frac{N_{grain} * {D_{mean}}^2}{MG_{area}} \tag{6}$$

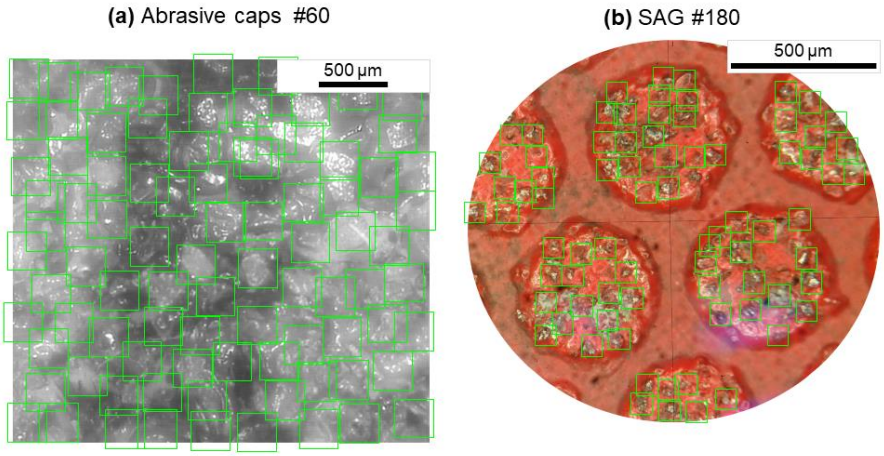

Fig. 11: Micro-graphs of polishing tools used to estimate the proportion of active grains: a) abrasive caps with #60 grits, b) shape adaptive grinding pellets with #180 grits. Active grains are shown in green.

4.2. Estimation of grain probability distribution considering tool wear: *k*

Initial grain distribution is defined as a Gaussian truncated by a maximum value (see section 3.3). Zhou et al. [22] proposed to represent tool wear by shifting the truncation of this Gaussian distribution. In that study, a grinding case was considered in which the largest grains are pulled out of the wheel first. Fig. 12 represents the Gaussian distribution of grains and truncation proposed by Zhou et al., using a parameter *Z* that crops the distribution leftward as larger grits are preferentially pulled out. However, Zhou's method only relates to the tool topography at a specific time in the wear process, and does not propose an equation for evolution as function of tool wear time.

In this present work, the Z parameter for truncation is replaced with the standard deviation of the mean grain value scaled by a factor *k* (Eq. 1). Furthermore, an expression representing evolution of the truncation as a function of time is proposed to reflect variation of *k* between an initial value k_0 and worn value k_1 (Eq. 7).

$$k(t) = k_1 * \ln(t+1) + k_0 \quad (7)$$

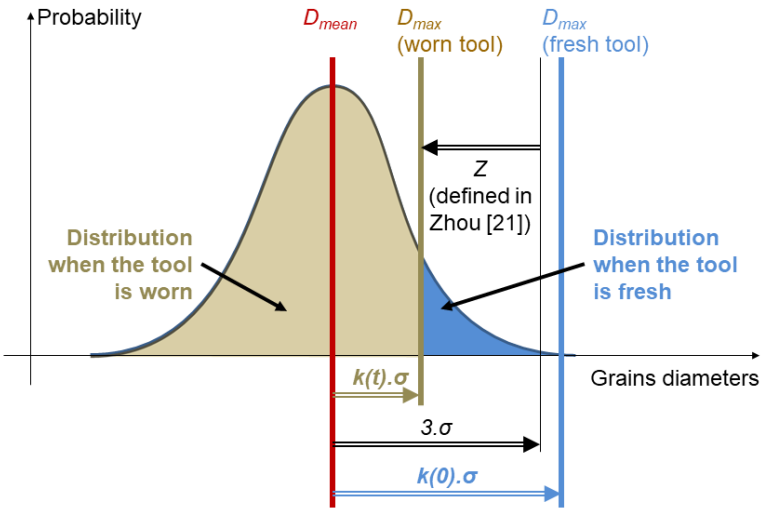

Fig. 12: Truncation of Gaussian grain distribution taking into account the tool wear.

To validate this model, experimental observations were carried out on two types of tools: abrasive caps and SAG. In the first experiment, the topography of an abrasive cap was measured with a scanning confocal chromatic probe at various stage of use (between 1 and 5 min). The 3D measurements were then processed by fitting spheres of radii equivalent to the grits (Fig. 13). Darker shades for the spheres indicate grains lost at an earlier stage of processing, and it is thus apparent that larger grits are pulled out earlier. The weak bonding bridges between grains in abrasive caps is insufficient to retain these larger abrasives within the tool matrix. In this observed case, the scale factor *k* varied between 10 and -2 (indicating that more than half the Gaussian distribution is cropped).

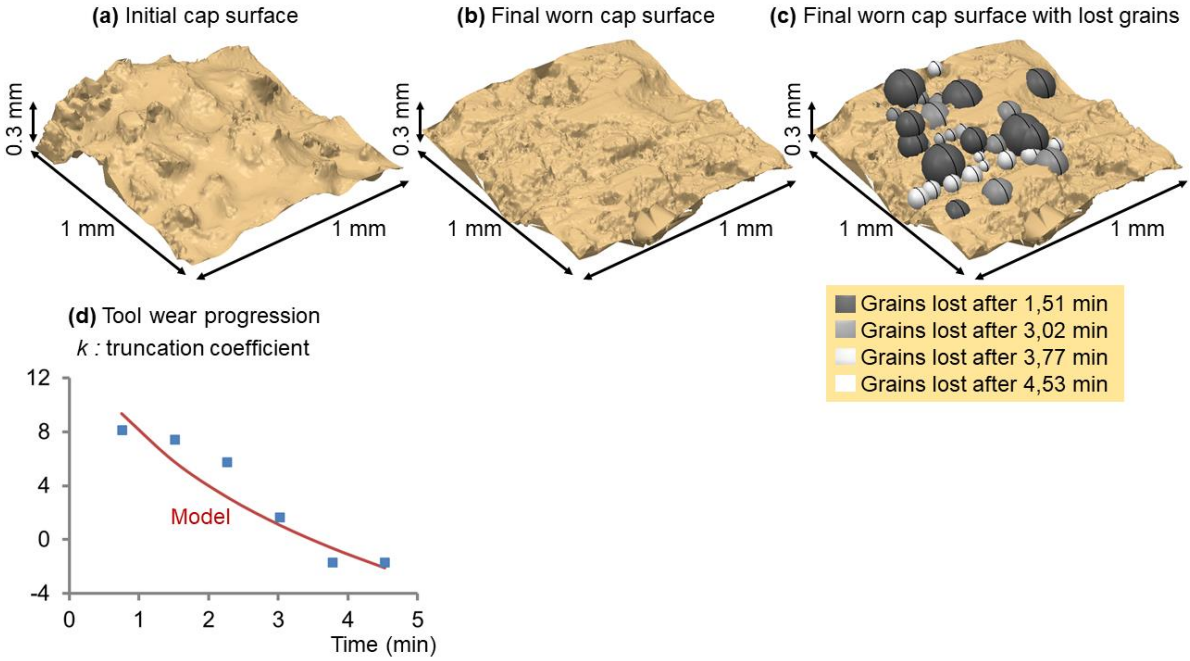

Fig. 13: Validation of proposed tool wear model on abrasive caps by measurement of same area of a tool at various stages of wear. 1x1 mm measurements show the surface of a) new tool, and b) fully worn tool. c) Superposition of lost grains as spheres on the worn tool (colour of spheres depends on the loss stage). d) Evolution of *k* truncation factor versus polishing time (tool wear).

In the second experiment, the topography of a SAG pellet was measured by scanning confocal laser microscope at various stages of use (between 1 and 10 hrs). The grits were identified and fitted with discs of equivalent cross-section area, with the yellow colour representing grains lost through the tool wear process (Fig. 14). While a few large grains disappeared, a greater loss affected grits at the lower end of the Gaussian distribution. Unlike cap tools, the nickel substrate used in SAG pellets shielded grains effectively such that only the tops of abrasives are contacting the workpiece surface. Therefore, large grains are deeply rooted in the bonding material and will remain affixed even as the pellet material slowly wears. With a measured tool binder wear rate of 1µm per hour, the binder shielding smaller grits is completely removed and these smaller grits will tend to be pulled out earlier in the process. In this observed case, the truncation factor *k* varied between -2 and -1.5.

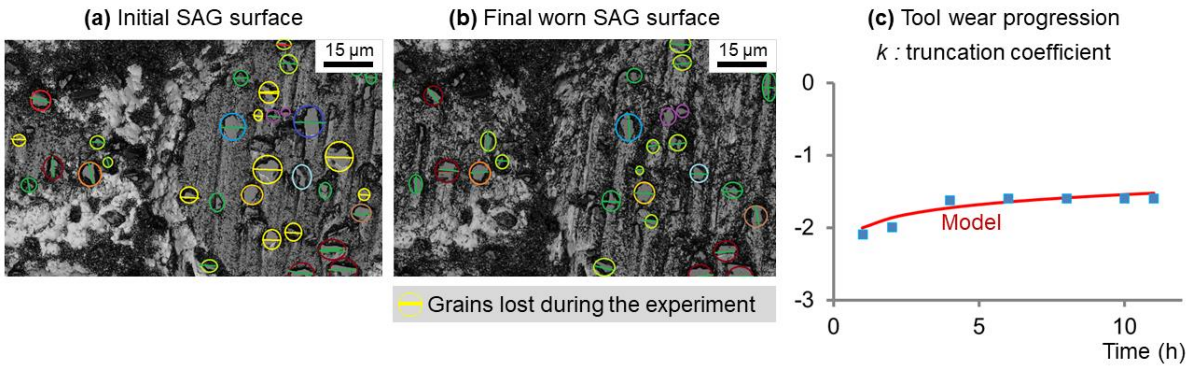

Fig. 14: Validation of proposed tool wear model for a shape adaptive grinding tool. a) Micrograph of the active zone of a new shape adaptive grinding tool with grains highlighted by coloured circles (colour depends on the grain diameter), b) Same area measured after several hours of polishing to determine the lost grains. c) Evolution of *k* truncation factor versus polishing time (tool wear).

5. Experimental validation

5.1. Sample definition

In order to validate the proposed method, a varied range of surface topologies and tool types were simulated and verified experimentally. For this purpose, a Selective Laser Melting (SLM) additive process was used to obtain a poor starting surface quality on rough workpieces. In this process, the quality of a surface may be influenced by the surface orientation relative to the support plane. With the aim to counter this issues, a sample composed of three planes (0°, 45° and 90°) covering the entire range of possible orientations relative to the plate was designed, as shown in Fig 15 a. The sample depth is 20 mm. Thereafter these three planes were continuously polished and the surface quality was recorded as the average of measurements performed on these three planes. All samples were produced with 17-4ph steel, which is a martensitic precipitation-hardening stainless steel.

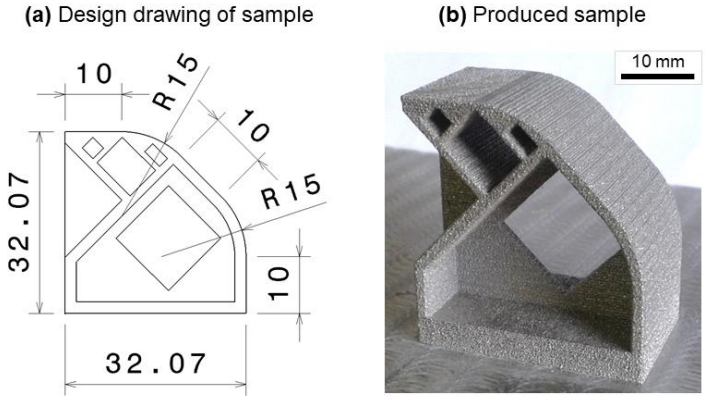

Fig 15: Workpiece used for experimental validation. (a) Workpiece design (b) Photograph of sample fabricated by Selective Laser Melting process

5.2. Definition of surface quality criteria

In the experimental validation, numerical criteria representing the three orders of defect are computed:

- Form (Pt): computed from the surfaces (3D measurement vs. pseudo 3D from simulated 2D profile), on which is applied a morphological filter with a 4 mm diameter virtual ball. This process emulates measurement of the surface by a common CMM with a high number of points. Next, the nominal surface is subtracted. The maximal amplitude of the residual error is recorded as form criterion ([32]).
- Waviness (Wa): computed using two successive Gaussian filters with cut-off length of 0.25 and 0.8 mm to conserve only the signal included between these two values. The obtained signal (measured vs. simulated) is used to compute the arithmetic mean deviation and provide the waviness criterion.
- Roughness (Ra): computed using a Gaussian filter with cut-off length of 0.25 mm to maintain the higher spatial frequency content of the signal. The obtained signal (measured vs. simulated) is used to compute the arithmetic mean deviation and provide the roughness criterion.

To quantify the surface quality of sample planes (0°, 45° and 90°), Sets of Points (SoP) were obtained through optical measurements using a chromatic confocal sensing Coordinate Measuring Machine (CMM) with a spot size of 4 µm:

- SoP1: 9x9 mm raster in steps of 50 µm in one direction, and 100 µm in the other.
- SoP2: 2x2 mm raster in steps of 4 µm in each direction.

The 3 criteria are derived from these two SoPs: The form criterion uses SoP1, whereas waviness and roughness criteria are computed from SoP2.

5.3. Machine types

In industry, polishing operations may be realized either on a dedicated polisher or milling machine. To be more general, both types of machines are employed to validate the proposed method, as shown in Fig. 16. First machine is a dedicated 7-axis polishing machine (located in Kyoto University, Japan). This kind of machine may independently control the position of the tool and the force it exerts on the polished surface. Second machine is a common 5-axis milling centre (located in Aix-Marseille University, France). These machines only control position, so flexibility of the tool was relied upon for a good balance between accurate contact force and tool positioning. The specifications of machine used for each experimental test are listed in Table 1.

(a) 7-axis polishing machine Zeeko IRP50

(b) 5-axis milling machine DMG US20

Fig. 16: Machine types used in the experimental validation. (a) Dedicated polisher (b) 5-axis milling machine.

5.4. Experiments and results

Four experiments were conducted, covering a wide range of surfaces topographies: form (St between [8, 120µm]), waviness (Sa_w between [0.1, 10µm]) and roughness (Sa_r between [0.05, 10µm]). In all experiments the surface considered in computation of the polishing path is a rectangular area 15 x 54 mm = 810 mm^2 (corresponding to the surface of the three planes and two corner radii as shown in Fig. 15). All toolpaths were rasters (parallel cross-sections) with a constant tool inclination relative to the surface normal. Table 1 presents the cutting parameters used for each stage, tool wear coefficient (see section 4.2), and active grain coefficient (section 4.1).

Table 1: Polishing tools and parameters used in experimental validation.

	CAP#60	CAP#320	SAG#180H	SAG#180L	SAG#1500	SAG#3000	W#240	F#5000
Machine	DMG	DMG	DMG	ZEEKO	ZEEKO	ZEEKO	DMG	DMG
Tool type	Abrasive cap #60	Abrasive cap #320	SAG* #180	SAG* #180	SAG* #1500	SAG* #3000	Flexible wheel#240	Felt #5000
Average grit size (µm)	280	45	80	80	9	3	58	1
Rotation per minutes (rpm)	12,000	12,000	12,000	1,500	1,500	1,500	12,000	2,000
Cutting speed (m/min)	555	555	258	32	32	32	1135	43
Feed rate (mm/min)	667	1000	920	200	300	150	500	500
Track spacing (mm)	0.5	0.15	0.2	0.1	0.18	0.2	0.15	0.15
Nominal tool offset (mm)	0.3	0.2	0.15	0.3	0.3	0.3	0.2	0.2
Tilt Angle (°)	60	60	20	20	20	20	20	20
Run-time for 810mm^2 (min)	2.43	5.4	4.4	40.5	15	27	10.8	10.8
Removal rate (mm^3/min)	46.04	35,3	6.8	0.85	0.0315	0.032	0.05	0.01
Tool footprint size (mm)	6	6	6	3	3	3	3	3
k **	3	5	3	3	3	3	5	3
p ***	1	1	4	4	4	4	10	10

* SAG: Shape adaptive grinding

** Number of standard deviation defining the maximum grain size

*** Tool type dependent coefficient accounting for density of active grains (density decreases when p increases).

5.4.1. Rough operations

In this section, polishing operations start directly from a rough SLM surface. This kind of surface has poor quality: form error of 0.12 mm, waviness and roughness around 10µm (average for the three 9x9 mm planar sections). The tested stage uses abrasive caps with grain size of 280 µm (noted CAP#60). Fig. 17 presents experimental and simulation results. In order to characterize the evolution of surface quality as a function of process time, five simulations and experiments were conducted for each stage whilst changing the feed rate by multiples of a base value (V_f=667 mm/min). The feed rate value directly affects the process time. Furthermore, error bars of two standard deviations were added to the experimental points (standard deviations are computed from sets of three 9x9 mm planar measurements). This figure brings to light accurate prediction of the three indicators of surface quality by the proposed method, in the case of a rough start condition. Furthermore, the intermediate simulated and experimental steps highlight one of the main interests of simulation, which is run-time optimisation of the polishing stage. For example, the orange simulation curve of

CAP#60 features a plateau which indicates that realising the same operation with double the feed rate (dividing by two the polishing time) would generate a similar surface quality. As this experiment validates the correct prediction of surface parameters as function of surface feed, further validation experiments were conducted for single feed values, without intermediate measurements.

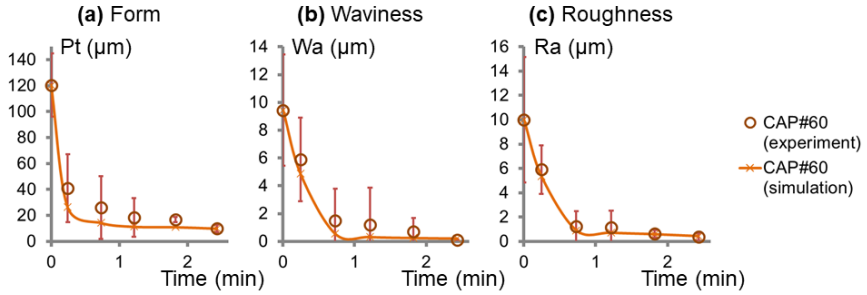

Fig. 17: Predicted and measured evolution of surface quality indicators against polishing time for CAP#60 stage (abrasive cap tool, grit number #60, 555 m/min). a) Form Pt, b) Waviness Wa, c) Roughness Ra.

5.4.2. Variation of cutting speed

In this experiment, variation of the cutting speed is tested on a rough SLM surface. SAG tool with grits of 80 µm are used in two experiments with different cutting speeds, one at 258 m/min and second at 32 m/min, respectively noted SAG#180H and SAG#180L in fig. 18. This spindle variation will influence the simulation in two respects: firstly the material removal rate (section 3.5, Eq. 4) and secondly the undistorted tool profile (section 3.3). Furthermore, it is interesting to note that these two stages are carried out on two different types of machines: SAG#180H on a milling machine and SAG#180L on a dedicated polisher machine (Fig. 16). As in section 5.4.1, error bars of two standard deviations were added on experimental points, and simulation results are composed of five simulations for interpolation purpose.

In Fig. 18, the SAG#180L progression curves appear as a distorted version of the SAG#180H curve, mainly due to reduction of the material removal rate. Contrary to the CAP#60 (Fig. 17), the green simulation curve of SAG#180L and SAG#180H are still sloping down, which means that the surface could be further improved by employing a slower feed rate. While this simple data analysis does not allow to clearly see the evolution of undistorted tool profile, section 6.2 below will delve on this point.

Once more, the simulation predicts accurately the surface quality criteria obtained experimentally. This experiment validates the usefulness of the method to predict process changes relating to cutting speed.

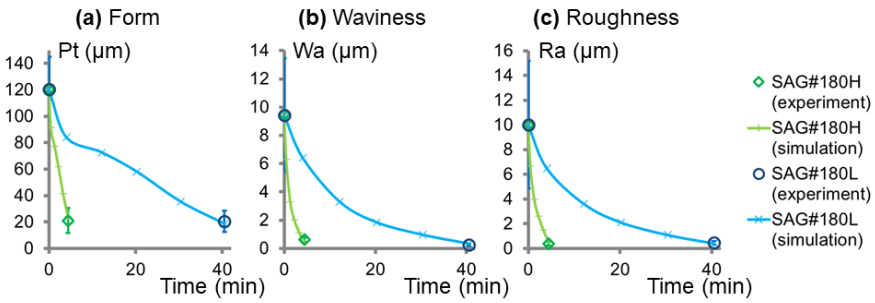

Fig. 18: Predicted and measured evolution of surface quality indicators against polishing time for SAG#180H (shape adaptive grinding tool, grit number #180, 258 m/min)

and SAG#180L (shape adaptive grinding tool, grit number #180, 32 m/min). a) Form Pt, b) Waviness Wa, c) Roughness Ra.

5.4.3. Sequence of similar tool types

In this experiment, two successive stages are tested on surfaces that have already received some prior polishing stage. Starting point corresponds respectively to form, waviness and roughness values of 8 µm, 0.37 µm and 0.33 µm. The first and second stages use a SAG tool, first with an average grit of 9 µm and second 3 µm (noted SAG#1500+SAG#3000 in fig. 19). In the model, the two simulated operations are chained by taking results of the first step as input into the second (noted SAG#1500 and SAG#3000 in fig. 19). Fig. 19 shows the good correlation between simulations and realised experiments, except for the roughness in SAG#3000 experiment. This discrepancy could not be explained by the standard deviation of the experiments. It must therefore be due to a limitation in the proposed model of SAG tool deformation when dealing with super-fine roughness. A more specific model is probably necessary for simulations involving roughness at the nanometre-level. Nevertheless, this experiment validates the usefulness of the method to predict the result of chained operations for identical tool types.

Furthermore, realised simulations/experiments highlight the difference in finishing between the SAG tool with 9 µm and 3 µm diameter diamonds. Results in Fig.19 show that these two types of operations have an insignificant influence on form. Meanwhile, the SAG#1500 tool has the property to significantly reduce both waviness and roughness very quickly. But the attainable roughness and waviness are limited by a plateau (around 0.05 µm Ra) that only a tool with a finer grain can reduce (SAG#3000).

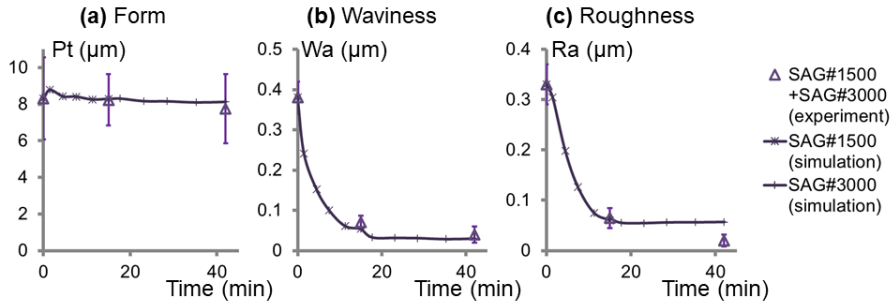

Fig. 19: Predicted and measured evolution of surface quality indicators against polishing time when processing in 2 steps with SAG#1500 (Shape Adaptive Grinding tools, grit number #1500, 32 m/min) and SAG#3000 (Shape Adaptive Grinding tools, grit number #3000, 32 m/min). a) Form Pt, b) Waviness Wa, c) Roughness Ra.

5.4.4. Sequence of different tool types

In this experiment, two different tool types are tested successively on surfaces that have received some prior polishing stage. Starting point corresponds respectively to form, waviness and roughness values of 8 µm, 0.14 µm and 0.25 µm. First tested stage uses a flexible wheel with an average grit of 58 µm (noted W#240), second a felt coated with alumina grains of 1 µm (noted W#240+F#5000 in Fig. 20). In these simulations, a slight oscillation may be observed in the roughness curve which can be explained by the repeatability level of simulations; indeed, error bars can be added to the simulation results. In the method implementation, a random undistorted tool profile is generated (see section 3.4). This profile will change even between two simulations with identical parameters. This variation is useful because it reflects the real stochastic variability between tools with identical nominal characteristics. This difference in tool profile may be completely neglected in rough polishing stage, but can have some influence in ultra-fine finishing operations. In Fig. 21, simulation error bars were shown for the wheel tool simulation in Fig. 20. Ten

simulations with identical parameters were carried out to obtain the standard deviation; the bars represent two standard deviations. On this figure only the roughness bars are presented because the standard deviation for the form and waviness results are negligible (respectively 0.08 µm and 0.0001 µm). The large standard deviation of the roughness results explain the small oscillations seen in Fig. 20). Nevertheless, this experiment validates the usefulness of the method to predict the chaining of operations with two different tool types.

On one hand, Fig. 20) shows that both wheel tools and felt tools are not particularly adapted to correcting form defects, because of their low stiffness. But on the other hand, unlike the felts, wheel tools are able to improve waviness defects. Another finding from Fig. 20) is that the plateau in roughness visible for F#5000 indicates that the polishing time may be significantly reduced.

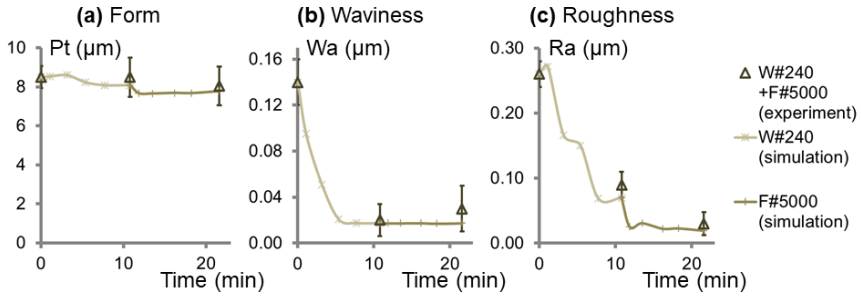

Fig. 20: Predicted and measured evolution of surface quality indicators against polishing time when processing in 2 steps with W#240 (Flexible wheel, grit number #240, 1,135 m/min) and F#5000 (Felt wheel, grit number #5000, 43 m/min). a) Form Pt, b) Waviness Wa, c) Roughness Ra.

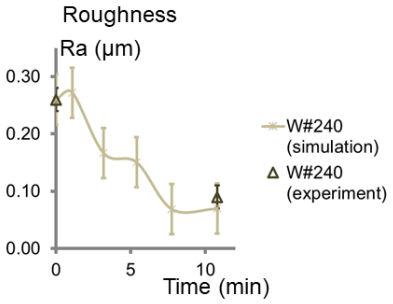

Fig. 21: Predicted and measured evolution of Roughness Ra against polishing time for W#240 (Flexible wheel, grit number #240, 1,135 m/min), with three standard deviation error bars calculated from repeat simulations.

6. Use of proposed method for a better understanding of finishing with compliant tools

6.1. Influence of polishing time on surface quality

Proposed method can quickly simulate a large number of polishing stages. These simulations may be used to visualize the influence of different polishing parameters on the obtained surface quality. Fig. 22 presents the results from different polishing simulations in the FS for the rough SLM surface (see section 5.4.1). These simulations compare seven polishing processes defined in table 1 with modulation of the feed rate. This modulation will directly impact the polishing time and the abrasion area (Eq. 7). In the simulation of stage

CAP#60, Fig. 22 a) helps to better understand the plateauing of form criterion mentioned in section 5.4.1. Indeed, as feed rate increases the material removal becomes more and more concentrated at the top of the peaks (corresponding to the cutting area in the FS, see section 3.6). Below a certain time (between [0.2, 0.41] min according to the simulation shown in Fig. 22 a), this removed material is not enough to supress entirely form defects from the rough SLM surface. Simulations provide an optimal value of 0.32 min to suppress these peaks with CAP#60. By comparison, processing by SAG#180H (Fig. 22 b) is not concentrated on the peaks but spread across a larger area. Consequentially, removal of the peaks is attenuated and it takes longer to attain the plateau in form defect improvement. Finally, other processes cannot reach this plateauing of form defects within an economically acceptable time. In the cases illustrated in Fig. 22, process W#240, F#5000, SAG#1500 and SAG#3000 are clearly not suitable to smooth out a rough SLM surface. From these simulations, general conclusions can be formulated for the different tool families (summarized in Table 2). In Fig. 22 a), cap tools are found to suppress form defect. From fig. 22 b), d), f) and g), SAG tools are not optimal for suppression of form defects, but offer an interesting solution to remove waviness error and improve surface roughness. From fig. 22 c) and e), wheels and felts cannot suppress large form and waviness error, and are therefore dedicated to improving roughness.

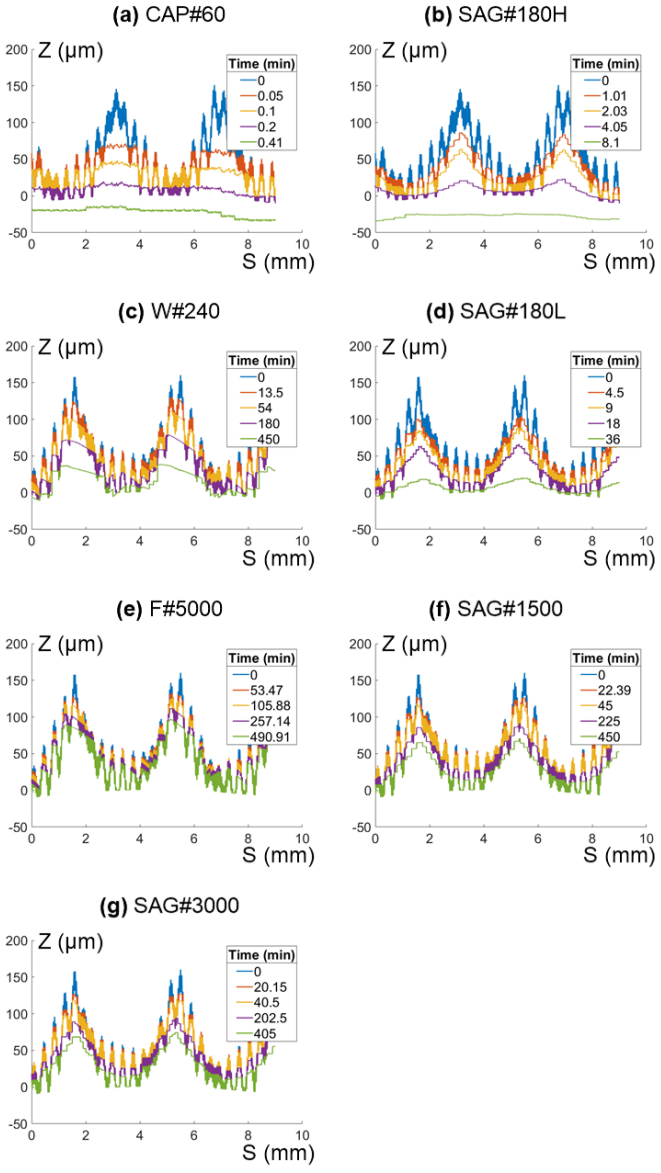

Fig. 22: Polishing simulations for various polishing tools and feed rates (polishing time calculated for 810 mm^2 area). Note: simulated polishing times differ between simulations. a) CAP#60 (abrasive cap tool, grit number #60, 555 m/min), b) SAG#180H, (shape adaptive grinding tool, grit number #180, 258 m/min) c) W#240 (flexible wheel, grit number #240, 1,135 m/min), d) SAG#180L (shape adaptive grinding tool, grit number #180, 32 m/min), e) F#5000 (felt wheel, grit size number #5000, 2,000 RPM), f) SAG#1500 (shape adaptive grinding tool, grit number #1500, 32 m/min) and g) SAG#3000 (shape adaptive grinding tool, grit number #3000, 32 m/min).

Table 2: Field of use of different tool families.

Tool families	Shape adaptive grinding	Abrasive caps	Flexible wheel	Felt
Target defect types	Waviness and roughness	Form	Roughness	Roughness

6.2. Influence of track spacing on the surface quality

In the previous section, the performance of various polishing processes was determined for a fixed track spacing. But the polishing time is in fact the product of the track spacing and feed rate. Thus, two identical processes with same overall polishing time (removing the same volume of material from the workpiece) but different values of track spacing are not expected to provide the same surface quality. Fig. 23 presents a simulation of CAP#60 with the appropriate polishing time for plateauing (determined in section 5.4.1), but with different sets of track spacing and feed rate. Two extrema curves (small track spacing with high feed rate, and large track spacing with low feed rate) are isolated for discussion, as shown in Fig. 23 b). This figure highlights that, for identical polishing time, a larger track spacing leads to more waviness defect but a better roughness (due to the low feed rate). Thus, it is possible through the simulations to select the optimum parameter set depending on whether the polishing step is meant to be a rough, intermediate or finishing stage.

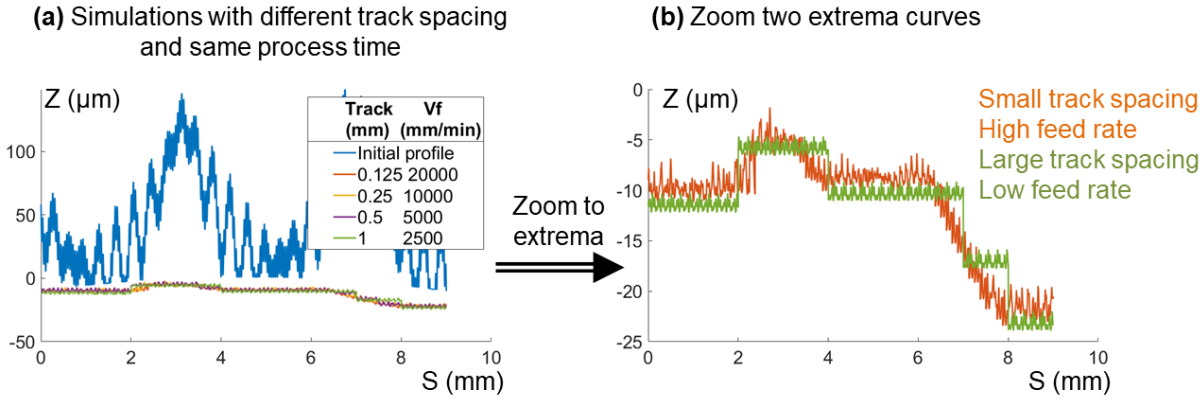

Fig. 23: Polishing simulations with CAP#60 (abrasive cap tool, grit number #60, 555 m/min) for identical process time but different track spacing. a) Initial surface profile and simulations conducted for 0.32 min of polishing at four different track spacing. b) Isolated extrema simulations (green: 1 mm spacing and Vf = 2,500 mm/min; red: 0.125 mm spacing and Vf = 20,000 mm/min)

6.3. Prediction of polishing process chains

Furthermore, the proposed method can serialize different polishing processes and predict the final polishing result. For instance, fig. 24 illustrates a 4-stage polishing process chain composed of an abrasive cap with large grains (Fig. 24 b) used to remove the bulk of

material, next a cap with small grains (Fig. 24 c) to finish suppressing form defect, followed by two successive SAG tools to achieve a fine surface roughness (Fig. 24 d) and e).

(a) Total process simulation

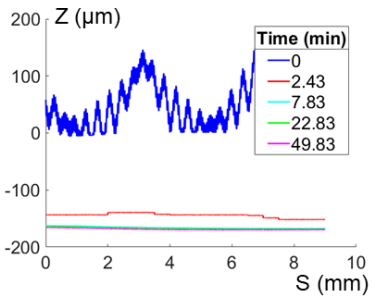

(b) Simulated polishing process chains:

	Tool type	Grit size number	Cutting speed (m/min)	Feed rate (mm/min)
Step1	Abrasive cap	#60	555	667
Step2	Abrasive cap	#320	555	1,000
Step3	Shape Adaptive Grinding	#1500	32	300
Step4	Shape Adaptive Grinding	#3000	32	150

(c) step1 **(d)** step2 **(e)** step3 **(f)** step4

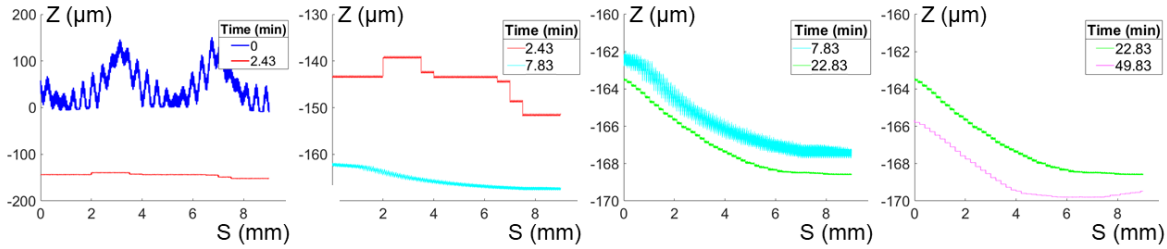

Fig. 24: Simulation of a 4-stage polishing process, a) initial and processed equivalent profiles, b) process chain definition, c) result of the first step by CAP#60 (abrasive cap tool, grit number #60, 555 m/min and feed rate 667 mm/min), d) result of the second step by CAP#320 (abrasive cap tool, grit number #320, 555 m/min and feed rate 1,000 mm/min), e) result of the third step by SAG#1500 (shape adaptive grinding tool, grit number #1500, 32 m/min and feed rate 300 mm/min)and f) result of the fourth step by SAG#3000 (shape adaptive grinding tool, grit number #3000, 32 m/min and feed rate 150 mm/min).

6.4. Sensitivity analysis

As previously mentioned in section 5.4.4, error bars can be added to the simulation results. Fig. 25 and 26 present the same SAG#3000 and F#5000 curves as in Fig. 19 and 20, but with simulation error bars added (two standard deviations). Furthermore, the standard deviation of experimental results obtained on the three different planes of the workpiece was also represented with error bars (see section 5.1).

On the one hand, in Fig. 25) the smalls deviations observed between simulations and experiments are mostly within these error bars. On the other hand, the deviation in roughness between the simulated and experimental test for SAG#3000 could not be explained by the standard deviations of the simulations and experiments. This highlights a limitation of the proposed model for SAG tools when dealing with super-fine roughness. As presented in [29], in their manufacture SAG tools undergo a conditioning stage that purposely induces a micro-flat on the grains so as to improve material removal stability. Such wear flat is not represented in the grain model, which is based on circles. Therefore, a more specific model is probably necessary for simulations involving roughness at the nanometre-level using SAG tools.

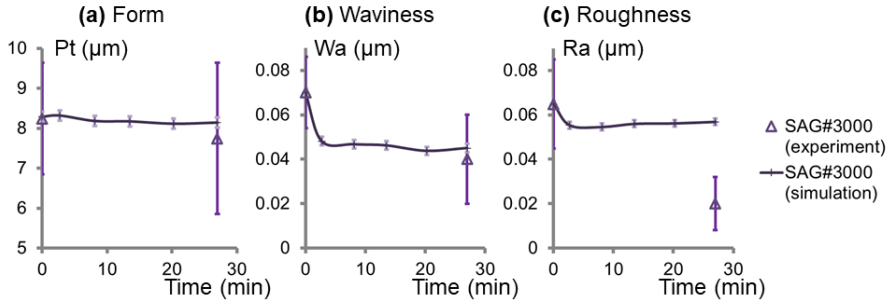

Fig. 25: Predicted and measured evolution of surface quality indicators against polishing time for SAG#3000 (shape adaptive grinding tools, grit number #3000, 32 m/min), with error bars added for repeat simulations. a) Form Pt, b) Waviness Wa, c) Roughness Ra.

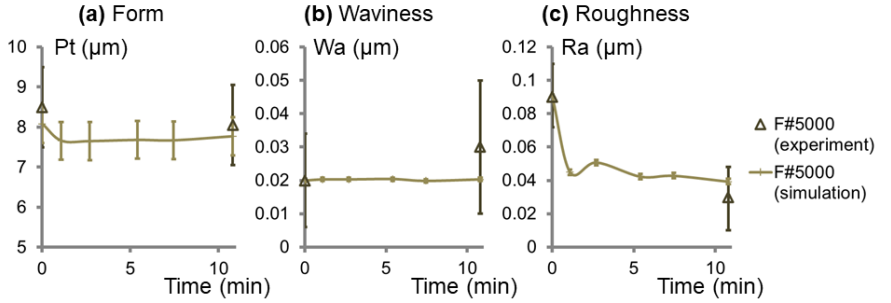

Fig. 26: Predicted and measured evolution of surface quality indicators against polishing time for F#5000 (felt wheel, grit number #5000, 43 m/min), with error bars added for repeat simulations. a) Form Pt, b) Waviness Wa, c) Roughness Ra.

6.5. Comparison with other analytical methods

As seen in the introduction, analytical methods to predict surface quality in finishing stage may be classified into three classes (Class #1, #2 and #3). Recall that Class #1 only considers the nominal tool shape, and Class #2 models the tool as an envelope profile of higher grains. These two models are implemented here and will be compared with the proposed method. Fig. 27 presents the results of simulations carried out for the SAG#180H tool and its associated parameters in table 1. The following observations are made:

- The Class #1 simulation produces a succession of arcs (of radius equal to that of the tool) distanced from each other by the track spacing value. Furthermore, the vertical position of this line is arbitrary since material removal rate is not taken into account. This model may be useful to estimate the obtained roughness with rigid tools (*e.g.* milling operation), but is clearly not suitable for the prediction of waviness and form.

- The Class #2 simulation results in a succession of small circles representing the active grains in a single tool rotation. Similarly to Class #1, the vertical position is defined arbitrarily. This model is more accurate than Class #1 in predicting the roughness in polishing or grinding, but is again not appropriate for waviness and form prediction.

- Proposed method is very different from the other two simulations because the time-dependent nature of the finishing process with compliant tool is considered (modulation of the material removal amount). The evolution of the surface profile is represented here for three different simulation times. This feature offers the opportunity to observe the evolution of form and waviness over time. Furthermore, unlike Class #2, the tool profile may deform to adapt to the local surface shape. This adaptation of the tool profile allows for coupling of waviness and roughness to be reflected in the process simulation. In summary, the proposed method is suitable to model the evolution of all surface quality parameters: form, waviness and roughness. And coupling effects in the surface generation at these three levels can be

computed within the same simulation (thanks to the use of FS which preserves all levels of surface defects and process characteristics).

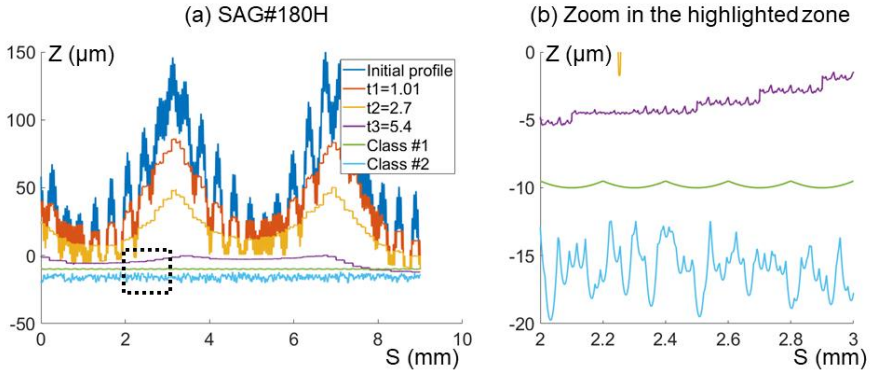

Fig. 27: a) Comparison between proposed model (for polishing times: t1=1.01, t2=2.7 and t3=5.4 min) and Class #1 (nominal tool shape) and Class #2 (tool envelope profile of higher grains in one revolution) models. Comparison was carried out for a rough selective laser melting surface and with SAG#180H (shape adaptive grinding tool, grit number #180, 258 m/min).

6.6. Limits of the proposed method

Although the proposed method is useful in predicting the evolution of surface quality criteria with high accuracy, it is not appropriate for prediction of the final topography of finished surfaces. Conducting simulations in a FS reduces drastically the simulation time, but it also reduces all 3D surface information to a 2D profile. As the relationship between the original surface and FS profile is not bijective, an infinity of 3D surfaces may share the same 2D equivalent profile. Thus, a complex 5-axis toolpath controlling the tool direction would produce the same simulated result as a more simple raster toolpath. Examples of such complex toolpaths include: the continuous precessing proposed by Beaucamp *et al.* [33] in which rotation of the tool axis around the local normal reduces surface roughness; the swing precess bonnet proposed by Cao et al. [34] which induces patterns and structures on the surface; the looping toolpath proposed by Chaves-Jacob et al. [35] that promotes homogeneous tool wear and surface coverage. The proposed simulation method is not capable of distinguishing between such cases.

Another limit of the proposed method resides in the determination of coefficients and parameters (see section 4), which may be slow and tedious if the tool manufacturer does not provide an accurate and detailed specification of the tools. Erroneous parameter selection can have a great influence on the obtained result.

Finally, in the case of super-fine roughness prediction (section 6.4) a limitation of the grain model (based on circles) was found with respect to SAG tools, while it did not affect felt tools. This difference may be explained by the conditioning of SAG tools by the manufacturer, which produces a micro-flat. This particular example shows that an accurate knowledge of all tool characteristics is necessary to attain accurate simulation.

7. Conclusion

In this paper, a method that can simulate and predict the geometrical results of compliant finishing operations was presented. This method performs the modelling of these operations in a Folding Space (FS), by merging the 3D surface topography information to a 2D space through the use of preferential directions relating to surface and process features. This approach is particularly well suited for compliant finishing processes, as the coupling between different levels of defect is reflected in the use of a deformed tool profile. This

approach also drastically reduces computation time (typically under 10s). This reduction of simulation time allows for repetition and chaining of simulations, in order to reach a better understanding of the finishing stage with compliant tools. The mains contributions of this paper can be summarized as follows:

- The proposed method is comprehensive as it takes into account the initial surface quality, abrasive grain distribution (including evolution with tool wear), nominal tool offset (including evolution due to profile variation), cutting speed, feed rate, removal rate (recalculated as function of tool offset and cutting speed), as well as deformation of the tool (as function of the surface profile evolution throughout the simulation and tool type).
- Rather than relying on generation of empirical removal data for every possible combinations of tool offset and advance feed, this work derived a simple yet powerful synthesis formula based on Hertz and Preston's equations, for prediction of removal rate with all spherical compliant tools.
- It is recognized that all compliant tools are not equal, and do not necessarily fully conform to the workpiece surface and defects. The theoretical analysis shows that levels of compliance found across a wide range of actual tools can be brought down to 3 main types of geometrical adaptions.
- The speed of proposed method allows for large scale multiplication of simulation runs to analyse the variation of surface quality under finishing operations with parameter adjustments. For instance, simulations highlight that the surface quality, contrary to what is commonly thought, is not only linked to the polishing time. Results show that increase in the track spacing (with a modulation of the rate to maintain the process time) increases the waviness while reducing the roughness.
- This work identified that progressive tool wear must be accounted for in order to produce reliable predictions. This could be achieved through the formulation of time-dependent truncation of the Gaussian distribution.

The proposed method was implemented and validated for a wide range of experiments: different machine types (milling and dedicated polishing machine), tools with widely differing structure and stiffness, numerous cutting parameters, and chained process steps. In each case, predictions from the method were very close to experimental results. On the other hand, the main limitation is the loss of 3D topographical information. From the obtained profile, reverse engineered 3D surfaces only offer an approximation (folding operation is not bijective).

The final section of this paper gave insights into the performance of various tool types with regards to improving form, waviness, or roughness, and showed that this method can provide useful guidance when trying to determine suitable compliant finishing process chains. The speed of simulations (typically under 10s) makes it possible to test a large number of scenarios and quickly identify suitable cutting conditions, as well as the sequence of operations and tools. The described implementation also allows for stochastic and systematic evolution of tool and process parameters to be investigated, such as the impact of machine behaviour (i.e thermal effects, cornering effects, etc.) on the tool offset. This topic will be worth investigating in future work. Overall, the proposed method will offer new and exciting opportunities for the optimisation of compliant finishing processes in industry.

Acknowledgements

This work was supported by the Grant-in-Aid for Scientific Research No. 20K04192 from the Japan Society for Promotion of Science, the grant program for research and development from the OSG foundation, and a donation research fund from DMG Mori Seiki Co. The experimental equipment was funded by the European Community, French Ministry of Research and Education, Aix-Marseille Conurbation Community and Zeeko Ltd. The authors also acknowledge the contribution of Mr. Ken Takizawa, former student of Kyoto University, in running some of the polishing experiments.

Reference

[1] Lison D, Lauwerys R, Demedts M, Nemery B (1996) Experimental Research into the Pathogenesis of Cobalt/Hard Metal Lung Disease. European Respiratory Journal 9:1024–1028.

[2] Kakinuma Y, Igarashi K, Katsura S, Aoyama T (2013) Development of 5-axis Polishing Machine Capable of Simultaneous Trajectory, Posture, and Force Control. CIRP Annals – Manufacturing Technology 62:379–382.

[3] Nagata F, Hase T, Haga Z, Omoto M, Watanabe K (2007) CAD/CAM-based position/force controller for a mold polishing robot. Mechatronics 17:207–216.

[4] Deyang F, Yuwen S, Huapeng D (2014) Investigations on the Automatic Precision Polishing of Curved Surfaces Using a Five-Axis Machining Centre. International Journal of Advance Manufacturing Technology 72(9–12):1625–1637.

[5] Pessoles X, Tournier C (2009) Automatic Polishing Process of Plastic Injection Molds on a 5-Axis Milling Center. Journal of Materials Processing Technology 209:3665–3673.

[6] Chaves-Jacob J, Linares JM, Sprauel JM (2015) Control of the contact force in a pre-polishing operation of free-form surfaces realised with a 5-axis CNC machine. CIRP Annals - Manufacturing Technology 64:309–312.

[7] CHAVES-JACOB J, LINARES JM, SPRAUEL JM (2013) Improving tool wear and surface covering in polishing via toolpath optimization, Journal of Materials Processing Technology 213:1661-1668.

[8] Beaucamp A, Namba Y, Combrinck H, Charlton P, Freeman R (2014) Shape adaptive grinding of CVD silicon carbide. CIRP Annals - Manufacturing Technology 63:317–320.

[9] Zhu WL, Yang Y, Li HN, Axinte D, Beaucamp A (2019) Theoretical and experimental investigation of material removal mechanism in compliant shape adaptive grinding process. International Journal of Machine Tools and Manufacture 142: 76-97.

[10] Yang Y, Li H, Liao Z, Axinte D, Zhu W, Beaucamp A (2020) Controlling of compliant grinding for low-rigidity components. International Journal of Machine Tools and Manufacture, 152: 103543.

[11] Cheung CF, Kong LB, Ho LT, To S (2011) Modelling and simulation of structure surface generation using computer controlled ultra-precision polishing. Precision engineering 35:574-590.

[12] Lu A, Jin T, Liu Q, Guo Z, Qu, M., Luo, H., Han M (2019) Modeling and prediction of surface topography and surface roughness in dual-axis wheel polishing of optical glass. International Journal of Machine Tools and Manufacture, 137: 13-29.

[13] Hecker RL, Liang SY (2003) Predictive modeling of surface roughness in grinding. International Journal of Machine Tools and Manufacture, 43: 755-761.

[14] Heinzel C, Grimme D, Moisan A (2006) Modeling of surface generation in contour grinding of optical molds, CIRP Annals-Manufacturing Technology, 55: 581-584.

[15] Cooper WL, Lavine AS (2000) Grinding process size effect and kinematics numerical analysis, Journal of manufacturing science and engineering, 122: 59-69.

[16] Denkena B, de Leon L, Turger A, Behrens L (2010) Prediction of contact conditions and theoretical roughness in manufacturing of complex implants by toric grinding tools. International Journal of Machine Tools & Manufacture 50:630–636.

[17] Zhang J, Wang H, Senthil Kumar A, Mingsheng Jin M (2020) Experimental and theoretical study of internal finishing by a novel magnetically driven polishing tool. International Journal of Machine Tools and Manufacture153: 103552.

[18] Uhlmanna E, Koprowskia S, Weingaertnerc WL, Rolon DA (2016) Modelling and simulation of grinding processes with mounted points: Part II of II - Fast modelling method for workpiece surface prediction. CIRP conference on high performance cutting 46:603-606.

[19] Dinesh Setti D, Arrabiyeh PA, Kirsch B, Heintz M, Aurich JC (2020) Analytical and experimental investigations on the mechanisms of surface generation in micro grinding. International Journal of Machine Tools and Manufacture 149: 103489

[20] Darafon A, Warkentin A, Bauer R (2013) 3D metal removal simulation to determine uncut chip thickness, contact length, and surface finish in grinding. Orthopaedics and trauma 66:1715-1724.

[21] Zhang Y, Fang C, Huang G, Xu X (2018) Modeling and simulation of the distribution of undeformed chip thicknesses in surface grinding. International Journal of Machine Tools and Manufacture, 127:14-27.

[22] Zhou X, Xi F (2002) Modeling and predicting surface roughness of the grinding process. International Journal of Machine Tools & Manufacture 42:969-977.

[23] ISO 16610-61 (2015) Geometrical product specification (GPS) -- Filtration -- Part 61: Linear areal filters -- Gaussian filters.

[24] ISO 4287 (1997) Geometrical Product Specifications (GPS) — Surface texture: Profile method — Terms, definitions and surface texture parameters.

[25] ISO 25178-2 (2012) Geometrical product specifications (GPS) — Surface texture: Areal — Part 2: Terms, definitions and surface texture parameters.

[26] Liu Y, Warkentin A, Bauer R, Gong Y (2013) Investigation of different grain shapes and dressing to predict surface roughness in grinding using kinematic simulations. Precision Engineering 37:758-764.

[27] Normes francaise, Abrasifs appliques- Granulometrie. ISO 6344-1, ISO 6344-2 and ISO 6344-3.

[28] Xi F, Zhou D (2005) Modeling surface roughness in the stone polishing process. International Journal of Machine Tools & Manufacture 45: 365-372.

[29] Beaucamp A, Namba Y, Charlton P (2015) Process mechanism in shape adaptive grinding (SAG). Annals of the CIRP 64/1:305–308.

[30] Preston FW (1927) The theory and design of plate glass polishing machines. Journal of Glass Technology, 11(44): 214-256.

[31] Hertz H (1881) Ueber die beruhrung fester elastischer korper. Journal reine und angewandte Mathematik 92:156-171.

[32] ISO 1101 (2017) Geometrical product specifications (GPS) -- Geometrical tolerancing -- Tolerances of form, orientation, location and run-out

[33] Beaucamp A, Namba Y (2013) Super-smooth finishing of diamond turned hard X-ray molding dies by combined fluid jet and bonnet polishing. Annals of the CIRP 62/1:315-318

[34] Cao ZC, Cheung CF, Ho LT, Liu MY (2017) Theoretical and experimental investigation of surface generation inswing precess bonnet polishing of complex three-dimensional structured surfaces. Precision Engineering, 50 361–371.

[35] Chaves-Jacob J, LINARES JM, SPRAUEL JM (2013) Improving tool wear and surface covering in polishing via toolpath optimization. Journal of Materials Processing Technology, 213/10: 1661-1668.